Photoproduction of nitric oxide in seawater

Ye Tian[1,2,3], Gui–Peng Yang[1,2,3], Chun–Ying Liu[1,2,3], Pei–Feng Li[3], Hong–Tao Chen[1,2,3], Hermann W. Bange[4]

[1]Key Laboratory of Marine Chemistry Theory and Technology, Ministry of Education, Qingdao, 266100, China

[2]Laboratory for Marine Ecology and Environmental Science, Qingdao National Laboratory for Marine Science and Technology, Qingdao 266071, China

[3]College of Chemistry and Chemical Engineering, Ocean University of China, Qingdao, 266100, China

[4] GEOMAR Helmholtz–Zentrum für Ozeanforschung Kiel, Kiel, 24105, Germany

Correspondence to: Chun–ying Liu (roseliu@ouc.edu.cn) and Hong–Tao Chen (chenht@ouc.edu.cn)

Abstract. Nitric oxide (NO) is a short–lived intermediate of the oceanic nitrogen cycle. However, our knowledge about its production and consumption pathways in oceanic environments is rudimentary. In order to decipher the major factors affecting NO photochemical production, we irradiated artificial seawater samples as well as 31 natural surface seawater samples in laboratory experiments. The seawater samples were collected during a cruise to the western tropical North Pacific Ocean (WTNP, a N/S section from 36 ° to 2 °N along 146 °/143 °E with 6 and 12 stations, respectively, and a W/E section from 137 ° to 161 °E along the equator with 13 stations) from November 2015 to January 2016. NO photoproduction rates from dissolved nitrite in artificial seawater showed increasing trends with decreasing pH, increasing temperatures and increasing salinity. In contrast, NO photoproduction rates (average: $0.5 \pm 0.2 \times 10^{-12}$ mol L^{-1} s^{-1}) in the natural seawater samples from the WTNP did not show any correlations with pH, water temperature and salinity as well as dissolved inorganic nitrite concentrations. The flux induced by NO photoproduction in the WTNP (average: 13×10^{-12} mol m^{-2} s^{-1}) were significantly larger than the NO air–sea flux densities (average: 1.8×10^{-12} mol m^{-2} s^{-1}) indicating a further NO loss process in the surface layer.

1 Introduction

Nitric oxide (NO) is a short–lived intermediate of the oceanic nitrogen cycle, see e.g. Bange (2008) and Kuypers et al. (2018). There are only a few reports about oceanic NO determination method so far because of its reactivity (Zafiriou et al., 1980; Lutterbeck and Bange, 2015; Liu et al., 2017). NO is produced and consumed during various microbial processes such as nitrification, denitrification and

30 anammox (Schreiber et al., 2012; Kuypers et al., 2018). Moreover, it is known that both phytoplankton

31 and zooplankton can metabolize NO and are influenced by ambient (extracellular) NO concentrations

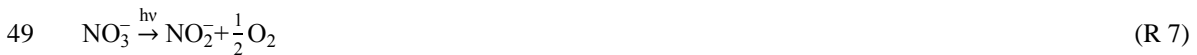32 (Singh and Lal, 2016; Wang et al., 2017; Astier et al., 2018).

33 Apart from (micro)biological processes, NO can be produced photochemically from dissolved nitrite

34 (NO_2^-) in the sunlit surface ocean (Zafiriou and True, 1979; Zafiriou and McFarland, 1981):

35 $NO_2^- + H_2O \xrightarrow{h\nu} NO + OH + OH^-$ (R 1)

36 Mack and Bolton (1999) had reviewed the possible subsequent reaction like the produced NO and

37 hydroxyl radical (OH) could react to produce HNO_2 reversely (R2), and some reaction that consumed

38 NO like R3 to R7

39 $NO + OH \rightarrow HNO_2$ (R 2)

40 $NO + NO_2 \rightarrow N_2O_3$ (R 3)

41 $N_2O_3 + H_2O \rightarrow 2H^+ + 2NO_2^-$ (R 3)

42 $NO + NO \rightarrow N_2O_2 + O_2 \rightarrow N_2O_4$ (R 4)

43 $2NO_2 \rightarrow N_2O_4$ (R 5)

44 $N_2O_4 + H_2O \rightarrow 2H^+ + NO_2^- + NO_3^-$ (R 6)

45 besides, in natural sunlit seawater, photolyzed dissolved nitrate (NO_3^-) could be a potential source of NO

46 through NO_2^- (R 8); during the process of ammonium (NH_4^+/NH_3) oxidation into NO_2^- and NO_3^-, NO

47 might be an intermedium (Joussotdubien and Kadiri, 1970), or NO could be produced through amino–

48 peroxyl radicals $(NH_2O_2^-)$ through R 8 to R 11 (Laszlo et al., 1998;Clarke et al., 2008)

49 $NO_3^- \xrightarrow{h\nu} NO_2^- + \frac{1}{2}O_2$ (R 7)

50 $OH^- + HCO_3^-/CO_3^{2-} \rightarrow CO_3^- + H_2O/OH^-$ (R 8)

51 $OH^- + NH_3 \rightarrow NH_2^- + H_2O$ (R 9)

52 $CO_3^- + NH_3 \rightarrow NH_2^- + HCO_3^-$ (R 10)

53 $NH_2^- + O_2 \rightarrow NH_2O_2^-$ (R 11)

54 $NH_2O_2^- \rightarrow NO^- + H_2O$ (R 12)

55 Table 1 summarized studies about photochemical production of NO measured in the surface waters of

56 the equatorial Pacific Ocean (Zafiriou et al., 1980; Zafiriou and McFarland, 1981), the Seto Inland Sea

57 (Olasehinde et al., 2009; Olasehinde et al., 2010; Anifowose and Sakugawa, 2017), the Bohai and Yellow

58 Seas(Liu et al., 2017; Tian et al., 2018) and the Kurose River (Japan) (Olasehinde et al., 2009; Anifowose

59 et al., 2015). NO photoproduction rates varied among different seawater samples, it seemed the rates in

60 Kurose River (average: 499×10^{-12} mol L^{-1} s^{-1}) was biggest, which was possibly due to an increase of

61 nitrite being released into the river in agricultural activity during the study time. However, NO

62 concentration was about 1.6×10^{-12} mol L^{-1}, at lowest level, which was because of higher scavenging

63 rate in river water (NO lifetime :0.25 s). The lifetime of NO showed increasing trend from river (several

64 seconds) to inland sea (dozens of seconds) to open sea (dozens to hundreds of seconds), reviewed in

65 Anifowose and Sakugawa (2017). However, NO showed higher concentration level in coastal waters

66 than in open sea, higher photoproduction rates might account for this.

67 In this study, we present the results of our measurements of NO photoproduction in laboratory

68 experiments using artificial and natural seawater samples. The major objectives of our studies were (i)

69 to decipher the factors affecting NO photoproduction in seawater, (ii) to determine the photoproduction

70 rates of NO from samples collected during a cruise to the western tropical North Pacific Ocean (WTNP)

71 and (iii) to quantify the role of photoproduction as a source of NO in the surface waters of the WTNP.

72 **2 Methods**

73 **2.1 Determination of dissolved NO in aqueous samples**

74 For the measurements of dissolved NO we applied the method described by Olasehinde et al. (2009): In

75 brief, NO in the aqueous samples was determined by trapping it with added 4,5–diaminofluorescein

76 (DAF–2, chromatographic grade from Sigma–Aldrich, USA) and measuring the reaction product

77 triazolofluorescein (DAF–2T) with a high performance liquid chromatography system (HPLC). We used

78 an Agilent 1260 Infinity HPLC (Agilent Technologies Inc., USA) system equipped with a Venusil XBP–

79 C18 column (5.0 μm; 4.6 mm × 250 mm i.d.). The column temperature was set to 25°C and the mobile

80 phase was comprised of acetonitrile (HPLC grade from Merck, Darmstadt, Germany) and phosphate

81 buffer (disodium hydrogen phosphate heptahydrate, guaranteed reagent from Sinopharm Chemical

82 Reagent Co., Ltd, Shanghai, China) solution (10 mmol L^{-1} at pH 7.4) with a ratio of 8:92 (*v:v*) and a

83 rate of 1 mL min^{-1} in the isocratic mode.

84 The injected sample volume was 5.0 μL. The eluate was analyzed with a fluorescence diode array

85 detector at wavelengths of 495 and 515 nm for excitation and emission, respectively. The retention time

86 of DAF–2T was about 5.5 min.

87　　An aliquot of 10 mL artificial seawater was bubbled with N_2 gas at a flow of 10 mL min^{-1} for 2 h to

88　　remove O_2 after 10 min of ultrasonic and heat degassing. The solution was then bubbled with high-purity

89　　NO gas (99.9 %, Dalian Date Gas Ltd., China) for 30 min. The concentration of the saturated NO stock

90　　solution was 1.4 mmol L^{-1}, which could be used within 3 h (Lantoine et al., 1995). A series of diluted

91　　NO solutions were prepared in N_2-purged water from the NO stock solution using a microsyringe (Xing

92　　et al., 2005; Liu et al., 2017). And the series samples were trapped by DAF-2 solution.

93　　The detection limit of dissolved NO in Milli–Q water was 9.0×10^{-11} mol L^{-1}, which was determined by

94　　S/N=3 (3×0.03) with the blank samples (n=7) and the slope (0.101) in the low concentration range (3.3

95　　$- 33 \times 10^{-10}$ mol L^{-1}). And average relative standard error of the NO measurements was +/− 5.7 % at a

96　　concentration of 3.0×10^{-9} mol L^{-1}.

97　　**2.2 Set–up of irradiation experiments**

98　　We performed irradiation experiments with Milli–Q water (18.2 MΩ cm, Millipore Company, USA),

99　　artificial seawater and natural seawater samples. Artificial seawater was prepared by dissolving 23.96 g

100　　NaCl, 5.08 g $MgCl_2$, 3.99 g Na_2SO_4, 1.12 g $CaCl_2$, 0.67 g KCl, 0.20 g $NaHCO_3$, 0.10 g KBr, 0.03 g

101　　H_3BO_3 and 0.03 g NaF in 1 L of Milli–Q water (Bajt et al., 1997) and filtered by 0.2 μm polyethersulfone

102　　membrane (Pall, USA) before the experiments.

103　　All irradiation experiments (except the experiments for the temperature dependence, see section below)

104　　were conducted at a constant temperature of 20 ℃ by controlling the temperature of thermostat water

105　　bath (LAUDA Dr. R. Wobser Gmbh & Co. KG, Germany). The height of cylindroid quartz cuvette used

106　　for irradiation was 70 mm and the inner diameter was 14 mm with the volume about 10 mL. The optical

107　　pathlength was about 70 mm. During the experiment, the quartz cuvette, filled with 10 mL sample and

108　　blocked by PTFE stopper, was installed in the simulator and a little higher than the water bath surface.

109　　All quartz cuvettes were treated in the same manner except the cuvettes wrapped in aluminum foil which

110　　served as dark control.

111　　Milli–Q water and artificial seawater samples were spiked with varying amounts of $NaNO_2$ (puriss. p.a.

112　　ACS grade from Sigma–Aldrich, USA; for details see sections below). All other chemicals were of

113　　analytical grade from Tianjin Kemiou Chemical Reagent Co., Ltd or Shanghai Sinopharm Chemical

114　　Reagent Co., Ltd.

115   Triplicate samples from each treatment were collected every 0.5 h with an entire irradiation time of 2 h.

116   At the sampling time, the SUNTEST CPS+ was turned off and triplicate subsamples were collected from

117   each sample in dark with microsyringe (50 μL), and then the cuvettes were quickly put back into the

118   water bath to continue the experiment until two hours.The data from the experiments with Milli–Q and

119   artificial seawater samples were fitted with a simple linear regression in artificial seawater samples (see

120   below). However, a linear relationship was not found > 30 min for the natural seawater samples, therefore,

121   we decided to choose 30 min as the total experimental time for natural seawater samples. Statistical

122   analyses were done using SPSS v.16.0 or Origin 9.0 and results were considered significant at $p \leq 0.05$.

123   The artificial light source was a 1.5 kW xenon lamp, which provided a light intensity of 765 W m^{-2}. The

124   lamp was installed in an immersion well photochemical reactor called SUNTEST CPS+ solar simulator

125   produced by ATLAS, Germany. The solar simulator employed in this study has been demonstrated to

126   produce spectra which mimics that of the solar radiation and emits a radiation of wavelength from 300

127   to 800 nm (Wu et al., 2015).

128   **2.3 Experimental outline**

129   **2.3.1 Optimal DAF–2 concentration and storage time**

130   In order to find out the optimal DAF–2 concentration, 10 mL of artificial seawater containing 0.5 μmol

131   L^{-1} NO$_2^-$ was irradiated with various concentrations of DAF–2 ranging from 0.7 μmol L^{-1} to 4.8 μmol

132   L^{-1} for 2 h.

133   To ascertain the sample storage time, 10 mL with artificial seawater samples containing 5.0 μmol L^{-1} or

134   0.5 μmol L^{-1} NO$_2^-$ were irradiated with various concentrations of DAF–2 for 2 h. After irradiation,

135   samples were kept in the dark and measured every 2 h.

136   **2.3.2 Influence of pH, temperature, salinity and wave lengths**

137   The influence of the pH was assessed by adjusting artificial seawater samples to pH levels of 7.1, 7.6

138   and 8.1 by addition of appropriate amounts of hydrochloric acid (2 mol L^{-1}) or caustic soda solution (2

139   mol L^{-1}).

140   To assess the influence of the temperature, artificial seawater samples were adjusted to temperatures of

141   10 ℃, 20 ℃ and 30 ℃ by controlling the temperature of the thermostat water bath.

142   To assess the influence of the salinity on the photoproduction of NO from dissolved NO_2^-, artificial

143   seawater samples were adjusted to different salinity of 20, 30 and 35 by adding Milli–Q water or NaCl

144   to the stock solution of artificial seawater.

145   In order to compare the contributions of ultraviolet A (UVA), ultraviolet B (UVB) and visible light to

146   the NO photoproduction, two kinds of light filter film were used (wrapped around the quartz cuvette

147   tubes: (i) a Mylar plastic film (from United States Plastic Cor., Lima, Ohio) which can only shield UVB

148   and (ii) a film, always used as car insulation film (from CPFilm Inc., USA) shielding both UVA and

149   UVB (Li et al., 2010;Wu et al., 2015).

150 **2.4 Calculations of photoproduction rates (R_{NO}), photoproduction rate constant (J_{NO}) and reaction**
151 **yield**

152   For the artificial seawater experiments determining the generation of NO from the NO_2^- photochemical

153   degradation, the data fitted with a simple linear regression with the form y = $R_{NO} \times t$ + b, where y is the

154   NO concentration which was calculated by the signal intensity of DAF–2T at time t and R_{NO} is the

155   photoproduction rate.

156   The photoproduction rate constant of NO from nitrite (J_{NO}) was determined by preparing different

157   concentrations of NO_2^- (0.5, 2.0 and 5.0 μmol L^{-1}) in Milli–Q water and artificial seawater. The slope of

158   the linear correlation between photoproduction rates and concentrations of NO_2^- represents J_{NO}

159   (Anifowose et al., 2015).

160   The yield of NO formation ($\%f_{NO}$) from the photodegradation via NO_2^- was estimated according to

161   Anifowose et al. (2015)

162     $\%f_{NO} = 100 \times J_{NO} \times c(NO_2^-) \times R_{NO}^{-1}$ (Eq 1)

163   where $c(NO_2^-)$ is the initial concentration of NO_2^-.

164 **2.5 Seawater samples**

165   Surface seawater samples were collected form a water depth of 1 m during a ship campaign to the western

166   tropical North Pacific Ocean on board the R/V "Dong Fang Hong 2" from 13 November 2015 to 5

167   January 2016. This cruise covered two sections: a N/S section from 36 to 2 °N along 146/143 °E with 6

168   and 12 stations, respectively, and a W/E section from 137 to 161 °E along the equator with 13 stations

169   (Fig. 1). Stations S0701 − S0723 were sampled between 11 and 28 November (i.e. the first part of the

170   N/S section), followed by sampling of W/E section between 16 and 27 December and sampling of

171   stations S0725 – S0735 between 30 December 2015 and 05 January 2016 (i.e. second part of the N/S

172   section). In addition, relevant surface currents are indicated in Fig. 1 (Fine et al., 1994; Zhao et al., 2016;

173   Zhang et al., 2018). The location of the Kuroshio Current on 15 November 2015 was taken from

174   https://www1.kaiho.mlit.go.jp/.

175   Seawater samples were collected using 8–liter Niskin bottles equipped with silicon O–rings and Teflon–

176   coated springs and mounted on a Sea–Bird CTD (conductivity, temperature, depth) instrument (Sea–Bird

177   Electronics, Inc., USA). A 750 mL black glass bottle was rinsed with in situ seawater three times, and

178   then was filled with seawater quickly through a siphon. When the overflowed sample reached the half

179   volume of the bottle, the siphon was withdrawn rapidly, and the bottle was sealed quickly. Samples were

180   filtered through 0.45 μm and 0.2 μm polyethersulfone membranes (Pall, USA) to minimize microbial

181   influence (Kieber et al., 1996; Yang et al., 2011). Then the filtered seawater was transferred in the dark

182   into acid–cleaned and pre–combusted amber glass bottles, stored in darkness at 4 ℃ and brought back to

183   the laboratory on land. Samples were re–filtered with 0.2 μm polyethersulfone membranes (Pall, USA)

184   before the irradiation experiments. DAF–2 solutions were added in the dark. The irradiation experiments

185   were conducted within two weeks after the samples arrived in the land laboratory, the maximum storage

186   time was about two months.

187   **2.6 Dissolved inorganic nitrogen (DIN) and pH measurements**

188   The concentrations of dissolved inorganic nitrogen (DIN = nitrate, nitrite, and ammonium) from the

189   cruise were analyzed using an automated nutrient analyzer (SKALAR San++ system, SKAlAR,

190   Netherlands) onboard. The detection limits were 0.05 μmol L^{-1} for nitrate, nitrite and ammonium. When

191   the concentration was below detection limit, $1/2$ of the detection limit (0.025 round-off to 0.02) was

192   used.

193   The pH values were measured just before the experiments by using a benchtop pH meter (Orion Star

194   A211, Thermo Scientific ™, USA) which was equipped with an Orion 8102 Ross combination pH

195   electrode (Thermo Scientific ™, USA). In order to ensure comparability with the temperature in the

196   irradiation experiments, pH values of the natural seawater samples were measured at 20 ℃. The pH meter

197   was calibrated with three NIST–traceable pH buffers (pH = 4.01, 7.00 and 10.01 at 20 ℃). The precision

198   of pH measurements was +/–0.01.

3 <mark>Results and Discussion</mark>

200 **3.1 Optimal DAF–2 concentration and storage time**

201 NO concentrations generated from photolysis of artificial seawater samples with an initial NO_2^-

202 concentration of 0.5 μmol L^{-1} increased with increasing DAF–2 concentrations and reached a maximum

203 at a DAF–2 concentration of 1.4 μmol L^{-1} (Fig. 2a). At DAF–2 concentrations >1.4 μmol L^{-1} no further

204 increase of the NO concentrations was observed. Thus, we used a DAF–2 concentration of 1.4 μmol L^{-1}

205 for all experiments.

206 Samples after reaction with DAF–2 and stored at 4 ℃ in the dark were stable for at least 28 h with the

207 measurement interval about 2 h (Fig. 2b). The relative standard deviations of the resulting NO

208 concentrations after irradiating samples containing 0.5 μmol L^{-1} and 5.0 μmol L^{-1} NO_2^- were +/– 13%

209 and +/– 7%, respectively. This demonstrated that photolysis samples with NO which were allowed to

210 react with DAF–2 could be stored for at least one day at 4 ℃ in the dark.

211 **3.2 Photoproduction of NO in Milli–Q water and artificial seawater**

212 The photoproduction rates of NO in samples with NO_2^- concentrations of 0.5, 2.0 and 5.0 μmol L^{-1} were

213 generally higher in artificial seawater than in Milli–Q water (Fig. 3a and 3b).

214 The resulting J_{NO} were 5.6 ±0.9 ×10^{-4} min^{-1} and 9.4 ±1.4 ×10^{-4} min^{-1} for Milli–Q water and artificial

215 seawater, respectively. They are lower than the J_{NO} of 34.2 ×10^{-4} min^{-1} for Milli–Q water reported by

216 Anifowose et al. (2015). The difference might be explained by different experimental set–ups such as

217 sample self–shading, in our study, the quartz cuvette was 70 mm height and inner diameter was 14 mm

218 with the volume about 10 mL while in Anifowose et al. (2015), the quartz photochemical reaction cell

219 was 3 cm in diameter, 1.5 cm in length, and had a 6.5 mL capacity.

220 **3.3 Influence of pH, temperature, salinity and wavelengths**

221 All irradiation experiments were conducted in artificial seawater with two different NO_2^- concentrations

222 of 0.5 and 5.0 μmol L^{-1}. The resulting NO concentrations were generally higher when irradiating the

223 samples with the initial NO_2^- concentration of 5.0 μmol L^{-1}. NO photoproduction rates showed

224 increasing trends with decreasing pH, increasing temperatures and increasing salinity, the relationship

225 between rates with salinity and temperature rates is significant ($p < 0.5$) (Fig. 4 and 5).

226 Reaction (1) indicates that decreasing pH which results in lower concentrations of OH^- which, in turn,

227 will promote NO formation via NO_2^-. This is in line with the finding of Li et al. (2011) who found that

228 the photodegradation rate of NO_2^- in Milli–Q water was higher at pH = 6.5 than at pH = 9.5. Tugaoen et

229 al. (2018) also found the effect of lowering pH to conjugate NO_2^- to HONO allowed for HONO

230 photolysis (pH = 2.5). Besides, higher pH could also inhibit N_2O_4 and N_2O_3 hydrolysis reaction (R4 and

231 R7) as reviewed by Mack and Bolton (1999). However in previous study of Chu and Anastasio (2007)

232 and Zellner et al. (1990), the quantum yield of OH (which equals to the quantum yield of NO) was

233 constant at the pH ranges from 6.0 to 8.0 and 5.0 to 9.0 under single wavelength light in nitrite solution.

234 This might indicated that decreasing pH in our study mainly reduced NO consumption rather than

235 increased NO production.

236 Higher temperatures led to increasing NO photoproduction rates according to the temperature

237 dependence of chemical reactions given by the Arrhenius formula:

238 $R = A \times \exp\left(-\frac{E}{R \times T}\right)$ (Eq 2)

239 where A is an Arrhenius prefactor and T is the temperature (K). This indicates that an increasing

240 temperature results in a higher rate, Chu and Anastasio (2007) also found that quantum yield of OH (or

241 NO) showed a decreasing trend from 295K, 263K to 240K. Moreover, this equation can be used to

242 consider the difference of the rates at two temperatures $T1$ and $T2$:

243 $R_{T2} = R_{T1} \times \exp\left(\frac{E}{R} \times \left(\frac{1}{T1} - \frac{1}{T2}\right)\right)$ (Eq 3)

244 If we assumed that E was a constant in the temperature ranges of 10 to 30 ℃ when $NO_2^- = 0.5$ μmol L^{-1},

245 and we plot ln R against $1/T$, we would get the E value as 57.5 kJ mol^{-1} K^{-1}. Using the photoproduction

246 rate at 20 ℃ (293.15 K) as our reference point ($T1$), an expression of the R_T with the temperature was as

247 follows:

248 $R_T = 2.7 \times 10^{-10} \times \exp\left(6920 \times \left(\frac{1}{293.15} - \frac{1}{T2}\right)\right)$ (Eq 4)

249 Similarly, we could conclude expression of the R_T with the temperature when $NO_2^- = 5.0$ μmol L^{-1},

250 $R_T = 7 \times 10^{-10} \times \exp\left(11026 \times \left(\frac{1}{293.15} - \frac{1}{T2}\right)\right)$ (Eq 5).

251 However, NO production rate at 0.5 μmol L^{-1} nitrite did not increase from 20 to 30 ℃, the plausible

252 explanation was that NO_2^- concentration here was the mainly influencing factor, NO_2^- might be run out

253 at 20 °C, if NO_2^- concentration increased, like up to 5.0 μmol L^{-1}, the temperature could make a noticeable

254 difference.

255 Higher salinity obviously enhanced photoproduction rates of NO in both Milli–Q water and artificial

256 seawater samples (with 0.5 μmol L^{-1} or 5.0 μmol L^{-1} initial NO_2^- concentrations). The regression

257 relationship is y = 0.37 x − 4.55 for 0.5 μmol L^{-1} NO_2^- and y=2.3 x − 39.5 for 5.0 μmol L^{-1} NO_2^-,

258 respectively, where x is the salinity (‰) and y is the photoproduction rate ($\times 10^{-10}$ mol L^{-1} s^{-1}). This result

259 indicates that with increasing ion strength NO production is enhanced, however, the exact mechanism is

260 unknown and need further study. Zafiriou and McFarland (1981) also demonstrated that artificial

261 seawater comprised with major and minor salts showed complex interactions. But Chu and Anastasio

262 (2007) reported that added Na_2SO_4 (4.0–7.0 mmol L^{-1}) in solution had no effect on the quantum yield of

263 OH.

264 The highest NO photoproduction rates were observed with full wave length band whereas the lowest NO

265 rates were observed with UVB. The NO photoproduction rates approached zero at wave lengths in the

266 visible band. The contribution of visible band, UVA band and UVB band were <1%, 30.7 %, 85.2 % and

267 <1.0 %, 34.2 %, 63.1 % for 0.5 and 5.0 μmol L^{-1} NO_2^-, respectively. Our results are in line with the

268 findings of Zafiriou and McFarland (1981) who found that samples exposed to (UV+visible) wave

269 lengths lost NO_2^- more rapidly than those exposed only to the visible wave lengths alone. Chu and

270 Anastasio (2007) found that under single wavelength light, quantum yield of OH decreased with the

271 wavelength (280 nm to 360 and plateau until 390) which meant that single wavelength light of UVB had

272 higher photoproduction rate than UVA. Since it might be because of the wild band of UVA (320–420

273 nm) that led to the summational higher rates under UVA than UVB (in our system 300-320). Moreover,

274 according to the UV–visible absorption spectra of NO_2^-, λ_{max} was 354 nm, which is in the range of UVA

275 (320–420 nm) (Zuo and Deng, 1998; Zafiriou and McFarland, 1981).

276 **3.4 Kinetics of the NO photoproduction**

277 The yields of NO formation from NO_2^- (%f_{NO}) in artificial seawater samples were about 70.1% and 97.9%

278 for the initial NO_2^- concentrations of 0.5 and 5.0 μmol L^{-1}, respectively. The missing NO yield (29.9%

279 for 0.5 μmol L^{-1} and 2.1% for 5.0 μmol L^{-1}) might result from NO production via other (unknown)

280 nitrogen–containing substrates (Anifowose et al., 2015). Another plausible explanation would be that

281 during the process of NO_2^- photoproduction, some NO were oxidized into NO_2, then NO_2 dimerized (R5)

10

282 and the dipolymer N_2O_4 would hydrolyze into NO_2^- and NO_3^- (R7), which actually reduce the

283 concentration of NO_2^- (Mack and Bolton, 1999).

284 Assuming a 100% yield from NO_2^- degradation and a fast reaction of NO with DAF–2 the observed

285 linear relationships during the various irradiation experiments (Fig. 6) indicate that NO photoproduction

286 was following a pseudo zero–order reaction. However, the R_{NO} ratios (average: 4.8) listed in Table 2

287 were not the same for the experiments despite the fact that the ratio of the initial NO_2^- concentrations (=

288 10) was the same for all experiments. This result, however, does point to reaction which is different from

289 a zero–order reaction.

3.5 Photoproduction rates of NO in the western tropical North Pacific Ocean

291 During the cruise surface temperatures and salinities were in the range from 22.15 ℃ to 30.19 ℃ and

292 34.57 to 35.05 respectively. The concentrations of NO_3^-, NH_4^+ and NO_2^- ranged from 0.03 μmol L^{-1} to

293 1.6 μmol L^{-1}, 0.20 μmol L^{-1} to 1.2 μmol L^{-1} and 0.02 μmol L^{-1} to 0.33 μmol L^{-1}, respectively (Fig. 6).

294 The measured photoproduction rates of NO ranged from 0.3 $\times 10^{-10}$ mol L^{-1} min^{-1} (station S0711) to 2.9

295 $\times 10^{-10}$ mol L^{-1} min^{-1} (station S0303), with an average value of 13.0 ± 7.6 $\times 10^{-11}$ mol L^{-1} min^{-1}.

296 Photoproduction rates did not show significant correlations with NO_2^-, NO_3^-, NH_4^+, pH, salinity, water

297 temperature as well as with colored dissolved organic matter (data not shown, the same method with Zhu

298 et al. (2017))(statistics computed with SPSS v.16.0).

299 The non–existing linear relationship between R_{NO} and dissolved NO_2^- during our cruise is in contrast to

300 the results of Olasehinde et al. (2010), Anifowose et al. (2015) and Anifowose and Sakugawa (2017)

301 who observed positive linear relationships between NO photoproduction rates and the NO_2^-

302 concentrations in the surface waters of the Seto Inland Sea and the Kurose River. This might because

303 that other factors like pH, salinity were different between samples collected at different stations.

304 In Table 1, we found that the average photoproduction rate of NO measured in our cruise is lower than

305 that of the Seto Inland Sea and the Kurose River which could be ascribed to higher background NO_2^- in

306 the inland sea waters (Olasehinde et al., 2009; 2010). Our result is slightly lower than the R_{NO} from the

307 central equatorial Pacific Ocean (> 10^{-12} mol L^{-1} s^{-1}), the lower concentration of NO_2^- (0.06 μmol L^{-1})

308 in our study area might account for this (Zafiriou and McFarland, 1981). In Table 1, the NO_2^-

309 concentration of 0.06 μmol L^{-1} in our study was lower than most of other study area like Qingdao coastal

310 waters (0.75 μmol L^{-1}) and the Seto Inland Sea (0-0.4 μmol L^{-1} or 0.5-2 μmol L^{-1}). In the study of

11

311   Anifowose et al. (2015), since the NO_2^- concentration of upstream K1 station was similar to ours (0.06

312    $\mu mol\ L^{-1}$), the higher R_{NO} might attributed to lower pH (7.36) as mentioned above.Or it might be because

313   the difference of the river water and the seawater, considering lower nitrite level of K1, dissolved organic

314   matter might also account for the higher R_{NO}. Because of its conservative mixing behavior with salinity,

315   dissolved organic matter always showed higher level in river than open sea (Zhu et al., 2017), which

316   could photodegrade itself to produce NO_2^-, finally to promote R_{NO}. In our study, the rates were adjusted

317   to the ambient conditions, which included nighttime samples when the rates were lower. From the T–S

318   diagram (Fig.7), we found that higher photoproduction rates at stations S0701 and S0704 might resulted

319   from the influence of the Kuroshio (see Fig. 1), with enhanced concentrations of NO_2^-. The higher NO

320   production rates measured for stations S0303/S0307 and S0717–S0723 might have been influenced by

321   the South Equatorial and North Equatorial Currents, respectively, but were obviously not associated with

322   enhanced NO_2^- concentrations.

323   If we take the missing 30% of f_{NO} in artificial seawater as the experimental error, then in our study, using

324   the J_{NO} in the artificial seawater, the average %f_{NO} value in natural water was calculated to be 52% (–

325   30%), indicating that there are other unknown nitrogenous compounds, for example, NO_2^- produced from

326   NO_3^- photolysis (R8) or from other organic matter which could further lead to NO production (Kieber et

327   al., 1999; Benedict et al., 2017; Goldstein and Rabani, 2007; Minero et al., 2007).

328   According to the photoproduction rates and the relevant NO_2^- in Olasehinde et al. (2010), Anifowose

329   and Sakugawa (2017) (Table 1), the photoproduction rates under lower than 0.02 $\mu mol\ L^{-1}$ NO_2^- might

330   not be determined in nearshore waters like the Seto Inland Sea.

331   **3.6 Flux densities of NO in the surface layer of the WTNP**

332   **3.6.1 Air–sea flux density of NO**

333   The NO flux densities were computed with (Eq 6):

334    $F = k_{sea}\,([NO] - pNO_{air} \times H^{cp})$ (Eq 6)

335    $pNO_{air} = x'NO_{air} \times (p_{ss} - p_w)$ (Eq 7)

336   here F stands for the flux density (mass area^{-1} time^{-1}) across the air–sea interface, k_{sea} is the gas transfer

337   velocity (length time^{-1}), [NO] is the measured concentration of NO in the surface seawater (mole volumn$^-$

338   ^{1}), x'NO_{air} is the mixing ratio of atmosphere NO (dimensionless). And p_{ss} is the barometric pressure

339   while p_w was calculated after Weiss and Price (1980):

340    $\ln p_w = 24.4543 - 6745.09/(T + 273.15) - 4.8489 \times \ln (T + 273.15)/100) - 0.000544 \times S)$ (Eq 8)

341   H^{cp} is the Henry's law constant which is calculated after Sander (2015) as:

342    $H^{cp}(T) = H^{\ominus} \times \exp (-\Delta sol\,H/R \times (1/T - 1/T^{\ominus})$ (Eq 9)

343   where $-\Delta sol\frac{H}{R} = \frac{dlnH}{dln(\frac{1}{T})}$, $H^{\ominus}$, and $-\Delta sol\,H/R$ are tabulated in Sander (2015) ($-\Delta sol\,H/R$=1600 and

344    $H^{\ominus}$=1.9×10^{-5} mol m^{-3} pa^{-1}). The reviewed several literatures about NO, $H^{\ominus}$ and the values in different

345   literatures were similar (Sander, 2015). In our calculation, the value in the Warneck and Williams (2012)

346   were used.

347   Then k_{sea} was calculated after (Wanninkhof, 2014) as (Eq 10),

348    $k_{sea} = k_w\,(1 - \gamma_a)$ (Eq 10)

349   γ_a is the fraction of the entire gas concentration gradient across the airside boundary layer as a fraction

350   of the entire gradient from the bulk water to the bulk air (dimensionless), k_a is the air side air-sea gas

351   transfer coefficient (length time^{-1}) according to (Mcgillis et al., 2000;Jähne et al., 1987;Sharqawy et al.,

352   2010), for the details of the calculation of k_w and γ_a see Tian et al. (2018).

353   Since onboard wind speeds were not available, ECMWF reanalysis data sets (ERA-5 hourly data) were

354   applied. We used a value of 10^{-11} (v/v) for atmospheric NO (Law, 2001). The atmosphere pressure was

355   set to 101.325 kPa.

356   Since the measurements [NO] were not available from the cruise we estimated [NO] by assuming that

357   (1) NO production is mainly resulting from NO_2^- photodegradation and (2) the NO photoproduction R_{NO}

358   as measured in our irradiation experiment is balanced by the NO scavenging rate R_s (3) rates of nitrite

359   photoproduction into NO was proportional to the irradiance flux in order to adjust the rates under

360   simulator light into ambient light at the sampling time (Zafiriou and McFarland, 1981; Olasehinde et al.,

361   2010):

362    $R_{NO} \times \frac{I_{ambient}}{I_{simulator}} = [NO] \times R_s,$ (Eq 11)

363   where R_s represents the sum of the rate constants for the scavenging compounds reacting with NO times

364   the concentrations of the scavenger compounds, $I_{ambient}$ and $I_{simulator}$ denote the light intensity of

365   the sampling station and the CPS+ simulator (765 W m^{-2}). $I_{ambient}$ was ECMWF reanalysis data sets

366   (ERA-5 hourly data, interpolation method). In the study of Zafiriou et al., (1980) and Anifowose and

367   Sakugawa, (2017), they reviewed the NO lifetime in the different area for the Kurose River (0.05–1.3 s),

368   the Seto Inland sea (1.8–20 s), and the central Equatorial Pacific (40-200 s, 170 °E Equatorial regions),

369   which showed an increasing trend from river to open sea. It seemed that NO life time in our study area

370   should be most similar to the central Equatorial Pacific. Considering part of our sampling stations were

371   in open sea while some stations were close to continent like New Guinea Island and Japan, average

372   lifetime about 100 s were applied in our study, however the uncertainty was not reported in the literature,

373   but estimated uncertainty about 30% might be appropriate. Tian et al (2018) found that NO concentration

374   in the surface water showed no significant difference with that in the bottom water (average depth: 43

375   m), so it seems reasonable to estimate the steady state NO concentration with the NO concentration in

376   the mixed layer. Then [NO] was estimated to range from 0 to 292×10^{-12} mol L^{-1} (0 means that sampling

377   time during nighttime), with an average of 49×10^{-12} mol L^{-1}, which was consistent with previous results

378   in central equatorial Pacific (46×10^{-12} mol L^{-1}), while it was lower than near continent seawater like the

379   Seto Inland Sea (up to 120×10^{-12} mol L^{-1}) and the Jiaozhou Bay (157×10^{-12} mol L^{-1}), which might be

380   because of higher nitrite concentration. NO showed lowest concentration in the Kurose River, which

381   might because of less nitrite, and shortest life time might also account for this in river water than in

382   seawater (Anifowose and Sakugawa, 2017).

383   In Table 1, the resulting flux density of NO for WTNP ranged from 0 to 13.9×10^{-12} mol m^{-2} s^{-1}, with an

384   average of 1.8×10^{-12} mol m^{-2} s^{-1}, which is in good agreement with that in central equatorial Pacific (see

385   Table 1) while it was lower than that in costal seawater such as the Seto Inland Sea or the Jiaozhou Bay,

386   consistent with NO concentration distribution.

387   **3.6.2 Oceanic photoproduction rates of NO**

388   The photoproduction rates from our irradiation experiments were extrapolated to the oceanic

389   photoproduction in the WTNP with the equation from (Bange and Uher, 2005; Uher and Andreae, 1996)

390    $$R_{ocean} = R_{NO} \times \left(\frac{I_{ocean}(1 - exp(-K_D \times MLD))}{I_{ss} \times K_D \times MLD} \right) \qquad \text{(Eq 12)}$$

391   where R_{ocean} and R_{NO} are the photoproduction rates for the ocean mixed layer and seawater irradiation

392   experiments, respectively, see Section 3.5. I_{ocean} and I_{ss} are the average global irradiance at the surface of

393   the ocean mixed layer and the solar simulator used here, K_D is the light attenuation coefficient and MLD

394   is the estimated mixed layer depth at the sampled station.

395   I_{ocean} was set to 185 W m^{-2}, while I_{ss} was 765 W m^{-2} in our study (Bange and Uher, 2005; Wu et al.,

396   2015). As described above, K_{D-354} was applied to estimate the MLD. In Smyth (2011), K_{D-340} to K_{D-380}

397   derived from 10% residual light level depths ranged from 0.04 m^{-1} to 0.07 m^{-1} for our study area, we used

14

398 the average value of 0.05. The MLD was taken as the layer depth where the temperature was 0.2 °C lower

399 than the 10 m near–face seawater layer (Montégut, 2004), ranging from 13 – 77 m with an average of 37

400 m. The resulting average R_{ocean} was about 8.6 $\pm$ 4.9 $\times 10^{-12}$ mol L^{-1} min^{-1} for the WTNP at the time of

401 our cruise. Besides, the temperature at 20 °C in our laboratory experiment would induce about 10% error

402 (Fig. 4e).

403 The flux induced by NO photoproduction in the WTNP (NO photoproduction rates divide by MLD,

404 average: 13 $\times 10^{-12}$ mol m^{-2} s^{-1}) were significantly larger than the NO air–sea flux densities (average:

405 1.8 $\times 10^{-12}$ mol m^{-2} s^{-1}) indicating a further NO loss process in the surface layer.

406 **Conclusion**

407 The results of our irradiation experiments showed that NO photoproduction from NO_2^- in artificial

408 seawater is significantly affected by changes in pH, temperature and salinity. We found increasing NO

409 production rates from dissolved NO_2^- with decreasing pH, increasing temperatures and increasing

410 salinity. In contrast we did not find any correlations of NO photoproduction with pH, salinity, water

411 temperature as well as dissolved NO_2^- in natural surface seawater samples from a cruise to the western

412 tropical North Pacific Ocean (November 2015 – January 2016). We conclude that the trends observed in

413 our irradiation experiments with artificial seawater do not seem to be representative for WTNP because

414 of the complex settings of open ocean environments. Moreover, we conclude that future changes of NO

415 photoproduction due to ongoing environmental changes such as ocean warming and acidification are,

416 therefore, difficult to predict and need to be tested by irradiation experiments of natural seawater samples

417 under varying conditions. The flux induced by NO photoproduction in the WTNP (average: 13 $\times 10^{-12}$

418 mol m^{-2} s^{-1}) were significantly larger than the NO air–sea flux densities (average: 1.8 $\times 10^{-12}$ mol m^{-2} s^{-}

419 ^{1}) indicating a further NO loss process in the surface layer. This indicates a further NO loss process in

420 the surface layer of the WTNP. In order to decipher and to quantify the NO production and consumption

421 pathways in the oceanic surface layer more comprehensive laboratory and onboard measurements are

422 required.

434   **References**

435   Anifowose, A. J., Takeda, K., and Sakugawa, H.: Photoformation rate, steady-state concentration and
436   lifetime of nitric oxide radical (NO·) in a eutrophic river in Higashi-Hiroshima, Japan,
437   Chemosphere, 119, 302-309, 2015.

438   Anifowose, A. J., and Sakugawa, H.: Determination of Daytime Flux of Nitric Oxide Radical (NO·) at
439   an Inland Sea-Atmospheric Boundary in Japan, J. Aquat. Pollut. Toxicol., 1, 1-6, 2017.

440   Astier, J., Jeandroz, S., and Wendehenne, D.: Nitric oxide synthase in plants: The surprise from algae,
441   Plant Sci., 268, 64-66, 2018.

442   Bajt, O., Šket, B., and Faganeli, J.: The aqueous photochemical transformation of acrylic acid, Mar.
443   Chem., 58, 255-259, 1997.

444   Bange, H. W., and Uher, G.: Photochemical production of methane in natural waters: implications for its
445   present and past oceanic source, Chemosphere, 58, 177-183, 2005.

446   Bange, H. W.: Gaseous Nitrogen Compounds (NO, N_2O, N_2, NH_3) in the Ocean, Elsevier 51–94 pp.,
447   2008.

448   Benedict, K. B., Mcfall, A. S., and Anastasio, C.: Quantum Yield of Nitrite from the Photolysis of
449   Aqueous Nitrate above 300 nm, Environ. Sci. Technol., 51, 4387-4395, 2017.

450   Chu, L., and Anastasio, C.: Temperature and wavelength dependence of nitrite photolysis in frozen and
451   aqueous solutions, Environ. Sci. Technol., 41, 3626-3632, 2007.

452   Clarke, K., Edge, R., Johnson, V., Land, E. J., Navaratnam, S., and Truscott, T. G.: The carbonate radical:
453   its reactivity with oxygen, ammonia, amino acids, and melanins, J. Phys. Chem. A, 112, 10147-
454   10151, 2008.

455 Fine, R. A., Lukas, R., Bingham, F. M., Warner, M. J., and Gammon, R. H.: The western equatorial
456   Pacific: A water mass crossroads, J. Geophys. Res.: Oceans, 99, 25063-25080, 1994.

457 Goldstein, S., and Rabani, J.: Mechanism of Nitrite Formation by Nitrate Photolysis in Aqueous
458   Solutions: The Role of Peroxynitrite, Nitrogen Dioxide, and Hydroxyl Radical, J. Am. Chem.
459   Soc., 129, 10597, 2007.

460 Jähne, B., Heinz, G., and Dietrich, W.: Measurement of the diffusion coefficients of sparingly soluble
461   gases in water, J. Geophys. Res.: Oceans, 92, 10767–10776, 1987.

462 Joussotdubien, J., and Kadiri, A.: Photosensitized Oxidation of Ammonia by Singlet Oxygen in Aqueous
463   Solution and in Seawater, Nature, 227, 700-701, 1970.

464 Kieber, D. J., Jiao, J., Kiene, R. P., and Bates, T. S.: Impact of dimethylsulfide photochemistry on methyl
465   sulfur cycling in the Equatorial Pacific Ocean, J. Geophys. Res.: Oceans, 101, 3715-3722, 1996.

466 Kieber, R. J., Li, A., and Seaton, P. J.: Production of nitrite from the photodegradation of dissolved
467   organic matter in natural waters, Environ. Sci. Technol., 33, 717-723, 1999.

468 Kuypers, M. M. M., Marchant, H. K., and Kartal, B.: The microbial nitrogen-cycling network, Nat. Rev.
469   Microbiol., 16, 263-276, 2018.

470 Lantoine, F., Trévin, S., Bedioui, F., and Devynck, J.: Selective and sensitive electrochemical
471   measurement of nitric oxide in aqueous solution: discussion and new results, J. Electroanal.
472   Chem., 392, 85-89, 1995.

473 Laszlo, B., Alfassi, Z. B., Neta, P., and Huie, R. E.: Kinetics and Mechanism of the Reaction of $\cdot NH_2$
474   with O_2 in Aqueous Solutions, J. Phys. Chem. A, 102, 8498-8504, 1998.

475 Law, C. S.: Air–sea transfer: N_2O, NO, CH_4 , CO, Encyclopedia of Ocean Sciences, 137-144, 2001.

476 Li, P. F., Li, W. S., Liu, C. Y., Zhu, X. C., and Zhang, Q.: The photodecomposition of nitrite in water (in
477   Chinese), Chin. J. Environ. Sci., 30, 1883-1888, 2011.

478 Li, Y., Mao, Y., Liu, G., Tachiev, G., Roelant, D., Feng, X., and Cai, Y.: Degradation of methylmercury
479   and its effects on mercury distribution and cycling in the Florida Everglades, Environ. Sci.
480   Technol., 44, 6661-6666, 2010.

481 Liu, C. Y., Feng, W. H., Tian, Y., Yang, G. P., Li, P. F., and Bange, H. W.: Determination of dissolved
482   nitric oxide in coastal waters of the Yellow Sea off Qingdao, Ocean Sci., 13, 623-632, 2017.

483 Lutterbeck, H. E., and Bange, H. W.: An improved method for the determination of dissolved nitric oxide
484   (NO) in seawater samples, Ocean Sci., 11, 959-981, 2015.

485 Mack, J., and Bolton, J. R.: Photochemistry of nitrite and nitrate in aqueous solution: a review, J.
486   Photochem. Photobiol., A, 128, 1-13, 1999.

487 Mcgillis, W. R., Dacey, J. W. H., Frew, N. M., Bock, E. J., and Nelson, R. K.: Water-air flux of
488   dimethylsulfide, J. Geophys. Res.: Oceans, 105, 1187–1193, 2000.

489 Minero, C., Chiron, S., Falletti, G., Maurino, V., Pelizzetti, E., Ajassa, R., Carlotti, M. E., and Vione, D.:
490   Photochemincal processes involving nitrite in surface water samples, Aquat. Sci., 69, 71-85,
491   2007.

492 Montégut, C. D. B.: Mixed layer depth over the global ocean: An examination of profile data and a
493   profile-based climatology, J. Geophys. Res.: Oceans, 109, -, 2004.

494 Olasehinde, E. F., Takeda, K., and Sakugawa, H.: Development of an analytical method for nitric oxide
495   radical determination in natural waters, Anal. Chem., 81, 6843-6850, 2009.

496 Olasehinde, E. F., Takeda, K., and Sakugawa, H.: Photochemical Production and Consumption
497   Mechanisms of Nitric Oxide in Seawater, Environ. Sci. Technol., 44, 8403-8408, 2010.

Sander, R.: Compilation of Henry's law constants (version 4.0) for water as solvent, Atmos. Chem. Phys., 14, 29615-30521, 2015.

Schreiber, F., Wunderlin, P., Udert, K. M., and Wells, G. F.: Nitric oxide and nitrous oxide turnover in natural and engineered microbial communities: biological pathways, chemical reactions, and novel technologies, Front. Microbiol., 3, 372, 2012.

Sharqawy, M. H., V, J. H. L., and Zubair, S. M.: Thermophysical properties of seawater: a review of existing correlations and data, Desalin. Water Treat., 16, 354-380, 2010.

Singh, V. K., and Lal, B.: Nitric oxide (NO) stimulates steroidogenesis and folliculogenesis in fish, Reproduction, 153, 133, 2016.

Smyth, T. J.: Penetration of UV irradiance into the global ocean, J. Geophys. Res.: Oceans, 116, 20-32, 2011.

Tian, Y., Xue, C., Liu, C. Y., Yang, G. P., Li, P. F., Feng, W. H., and Bange, H. W.: Nitric oxide (NO) in the Bohai and Yellow Seas, Biogeosciences Discuss.(DOI: 10.5194/bg-2018-446), 2018, 1-25, 2018.

Tugaoen, H. O. N., Herckes, P., Hristovski, K., and Westerhoff, P.: Influence of ultraviolet wavelengths on kinetics and selectivity for N-gases during TiO_2 photocatalytic reduction of nitrate, Appl. Catal., B, 220, 597-606, 2018.

Uher, G., and Andreae, M. O.: The diel cycle of carbonyl sulfide in marine surface waters: Field study results and a simple model, Aquatic Geochemistry, 2, 313-344, 1996.

Wang, B., Dan, L., Chao, W., Wang, Q., Hui, Z., Liu, G., Xia, T., and Zhang, L.: Mechanism of endothelial nitric oxide synthase phosphorylation and activation by tentacle extract from the jellyfish Cyanea capillata, Peerj, 5, e3172, 2017.

Wanninkhof, R.: Relationship between wind speed and gas exchange over the ocean revisited, Limnol. Oceanogr. Methods, 12, 351-362, 2014.

Weiss, R. F., and Price, B. A.: Nitrous oxide solubility in water and seawater, Mar. Chem., 8, 347-359, 1980.

Wu, X., Liu, C. Y., and Li, P. F.: Photochemical transformation of acrylic acid in seawater, Mar. Chem., 170, 29-36, 2015.

Xing, L., Zhang, Z. B., Liu, C. Y., Wu, Z. Z., and Lin, C.: Amperometric Detection of Nitric Oxide with Microsensor in the Medium of Seawater and Its Applications, Sensors, 5, 537-545, 2005.

Xue, C., Liu, C., Yang, G., Zhu, C., and Zhang, H.: Distribution and controlling factors of nitric oxide concentrations in surface seawater of Jiaozhou Bay and adjacent waters (in Chinese), Chin. J. Environ. Sci., 33, 1086-1090, 2012.

Yang, G. P., Ren, C. Y., Lu, X. L., Liu, C. Y., and Ding, H. B.: Distribution, flux, and photoproduction of carbon monoxide in the East China Sea and Yellow Sea in spring, J. Geophys. Res.: Oceans, 116, 1-15, 2011.

Zafiriou, O. C., and True, M. B.: Nitrite photolysis in seawater by sunlight ☆, Mar. Chem., 8, 33-42, 1979.

Zafiriou, O. C., Mcfarland, M., and Bromund, R. H.: Nitric oxide in seawater, Science, 207, 637, 1980.

Zafiriou, O. C., and McFarland, M.: Nitric oxide from nitrite photolysis in the central equatorial Pacific, J. Geophys. Res.: Oceans, 86, 3173–3182, 1981.

Zellner, R., Exner, M., and Herrmann, H.: Absolute OH quantum yields in the laser photolysis of nitrate, nitrite and dissolved H_2O_2 at 308 and 351 nm in the temperature range 278–353 K, J. Atmos. Chem., 10, 411-425, 1990.

542 Zhang, Z., Qiu, B., Tian, J., Zhao, W., and Huang, X.: Latitude-dependent finescale turbulent shear
543   generations in the Pacific tropical-extratropical upper ocean, Nat. Commun., 9, 4086, 2018.
544 Zhao, J., Li, Y., and Wang, F.: Seasonal variation of the surface North Equatorial Countercurrent (NECC)
545   in the western Pacific Ocean, Chin. J. Oceanol. Limnol., 34, 1332-1346, 2016.
546 Zhu, W. Z., Zhang, J., and Yang, G. P.: Mixing behavior and photobleaching of chromophoric dissolved
547   organic matter in the Changjiang River estuary and the adjacent East China Sea, Estuarine,
548   Coastal Shelf Sci., 2017.
549

550

551

552   **Fig. 1.** Locations of the sampling stations in the western tropical North Pacific Ocean. The acronyms

553   NGCC, SEC, NECC, NEC, and STCC stand for New Guinea Coastal Current, South Equatorial Current,

554   North Equatorial Counter Current, North Equatorial Current, and Subtropical Counter Current,

555   respectively.

556   **Fig. 2.** Changes of NO concentrations with initial DAF–2 concentration of 0, 0.7, 1.4, 2.1, 2.8, 3.5 and

557   4.2 µmol L^{-1} after irradiation time of 2 h (a) and changes of different NO concentrations with storage

558   time monitored at about 2 h time intervals (b).

559   **Fig. 3.** Photoproduction rates of NO with 0.5, 2, and 5.0 µmol L^{-1} NO_2^- (a) and the calculated J_{NO} values

560   in Milli–Q water and artificial seawater (b), symbols in red represented for the artificial seawater samples

561   and in black for Milli–Q water.

562   **Fig. 4.** NO concentration changes with irradiation time at different pH, salinity, temperature and

563   waveband conditions (a, c, e, g for 0.5 µmol L^{-1} NO_2^- and b, d, f, h for 5.0 µmol L^{-1} NO_2^-).

564   **Fig. 5.** Changes of NO photoproduction rates with irradiation time at different pH, salinity, temperature

565   and waveband conditions (a, c, e, g for 0.5 µmol L^{-1} NO_2^- and b, d, f, h for 5.0 µmol L^{-1} NO_2^-).

566   **Fig. 6.** Seawater temperature, salinity, concentrations of NO_2^-, NO_3^-, NH_4^+, and photoproduction rates

567   of NO (R_{NO}) in the western tropical North Pacific Ocean. (a: W/E transect; b: N/S transect)

568   **Fig. 7.** The potential temperature–salinity (T–S) diagram with NO photoproduction rates indicated in the

569   color bar. Water mass characteristics of surface currents shown in Figure 1 are indicated. The acronyms

570   NGCC, SEC, NECC, NEC, and STCC stand for New Guinea Coastal Current, South Equatorial Current,

571   North Equatorial Counter Current, North Equatorial Current, and Subtropical Counter Current,

572   respectively.

573

574

575

Fig. 1. Locations of the sampling stations in the western tropical North Pacific Ocean. The acronyms NGCC, SEC, NECC, NEC, and STCC stand for New Guinea Coastal Current, South Equatorial Current, North Equatorial Counter Current, North Equatorial Current, and Subtropical Counter Current, respectively.
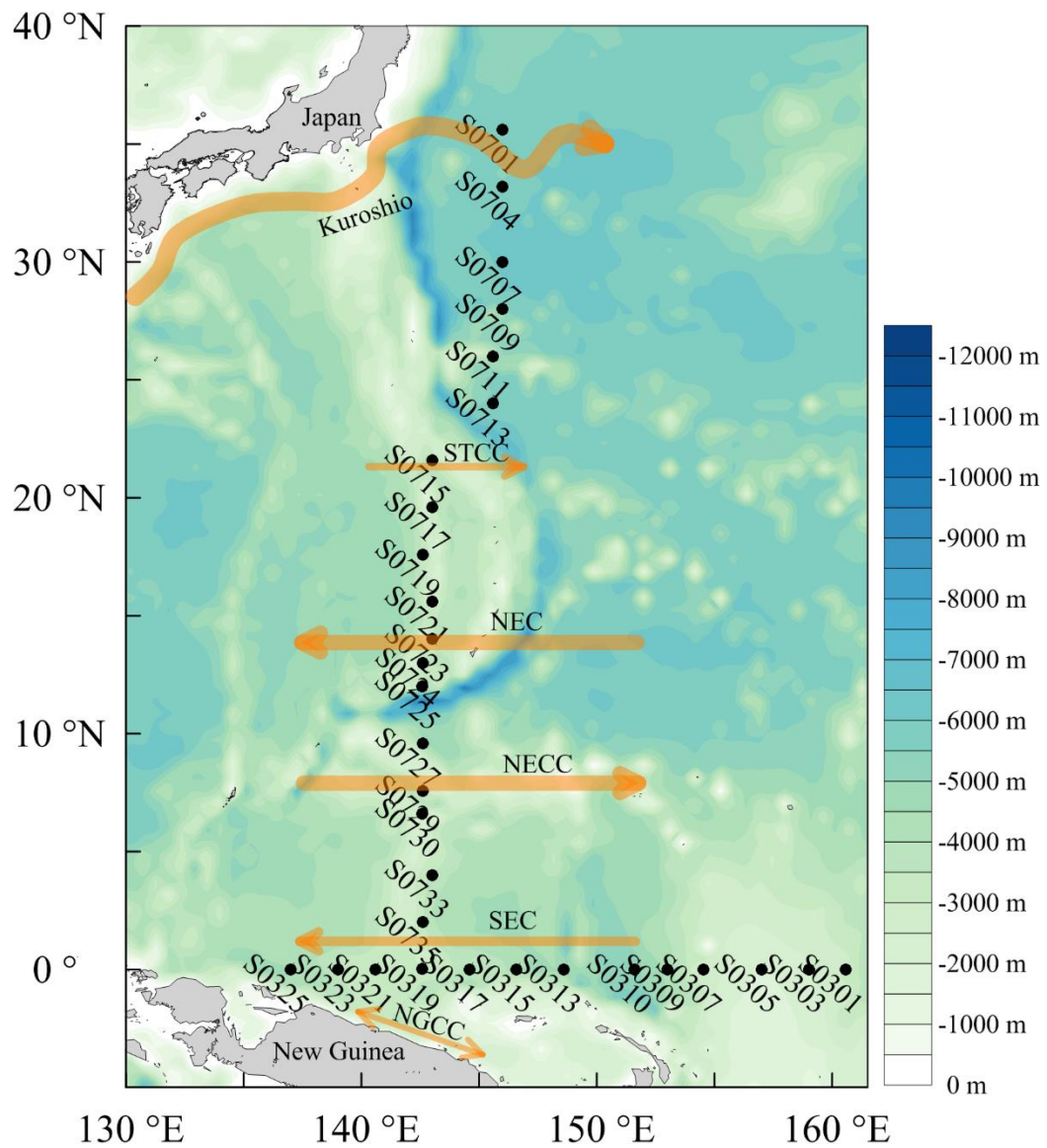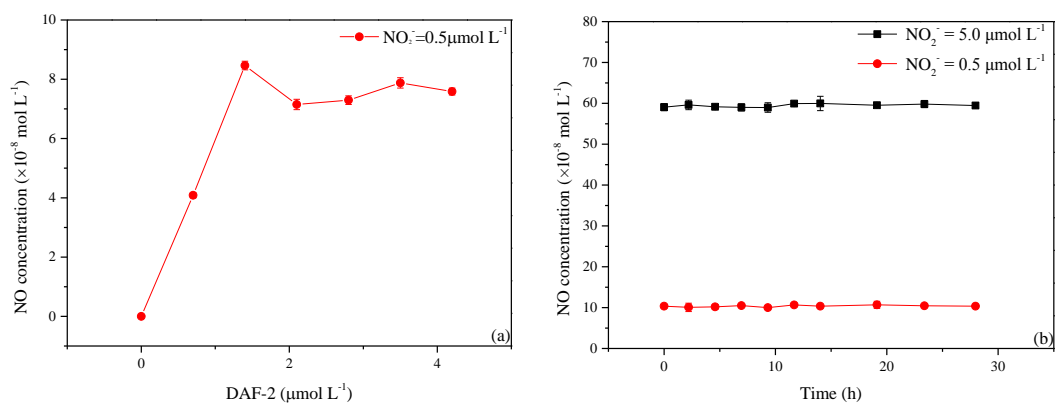
580

581

Fig. 2. Changes of NO concentrations with initial DAF–2 concentration of 0, 0.7, 1.4, 2.1, 2.8, 3.5 and

4.2 μmol L^{-1} after irradiation time of 2 h (a) and changes of different NO concentrations with storage

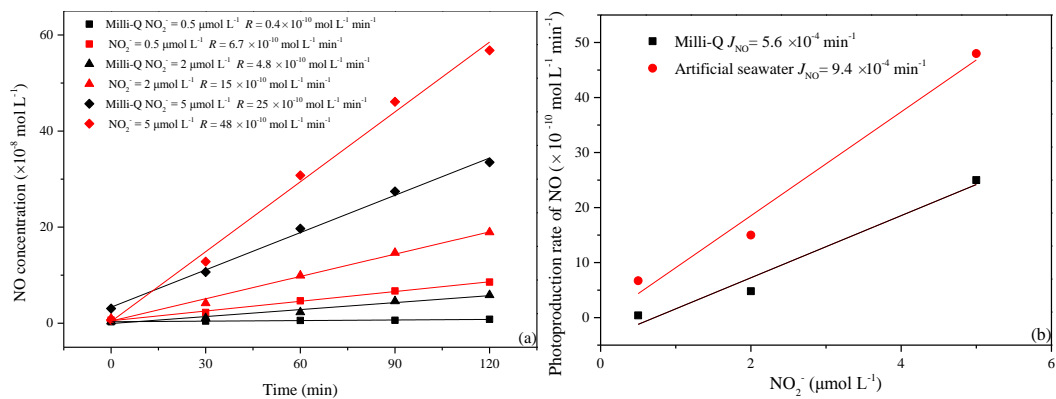time monitored at about 2 h time intervals (b).

585

586

587

588 **Fig. 3.** Photoproduction rates of NO with 0.5, 2, and 5.0 μmol L^{-1} NO$_2^-$ (a) and the calculated J_{NO}

589 values in Milli–Q water and artificial seawater (b), symbols in red represented for the artificial
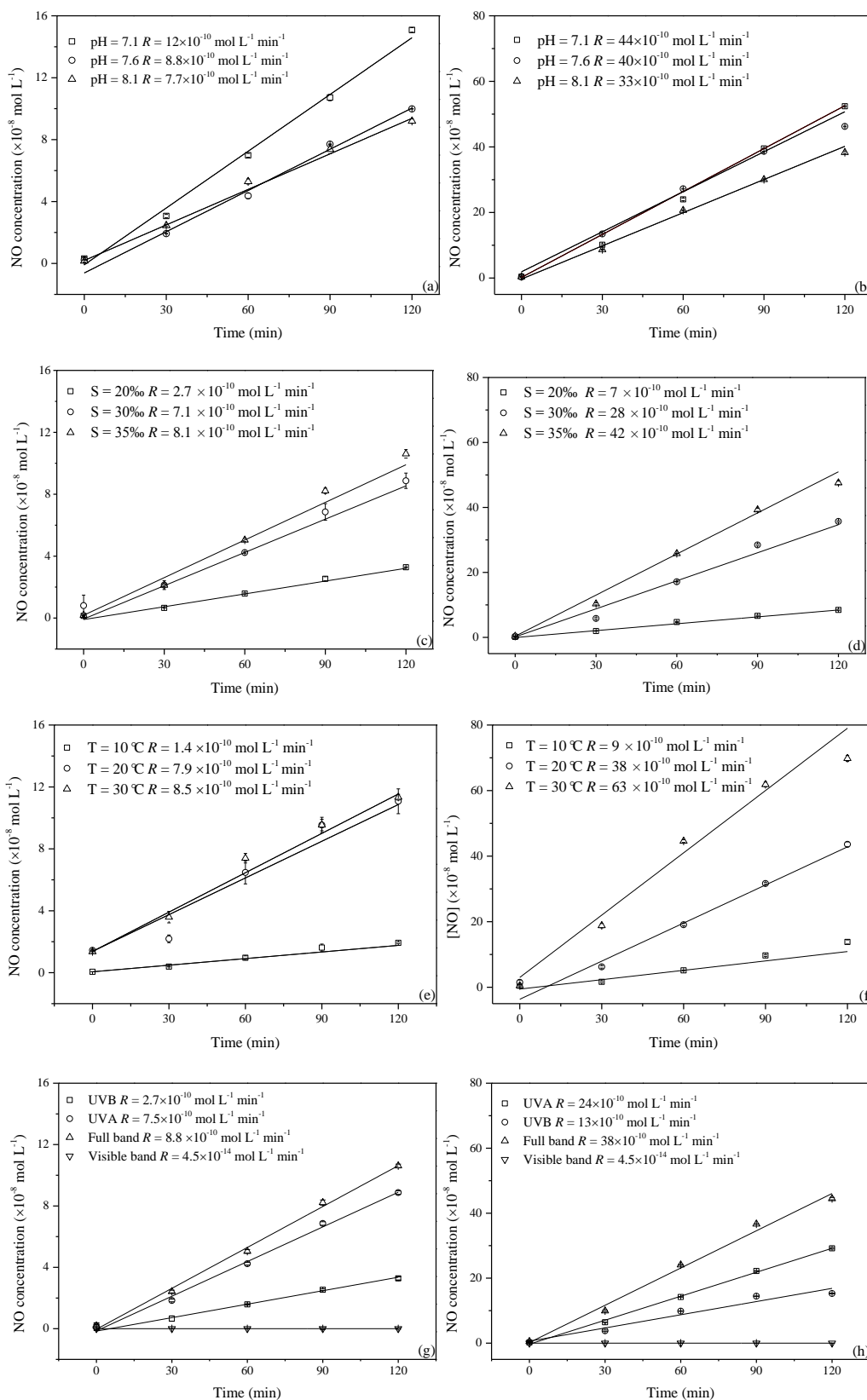
590 seawater samples and in black for Milli–Q water.

591

592

593

594

595

Fig. 4. NO concentration changes with irradiation time at different pH, salinity, temperature and

waveband conditions (a, c, e, g for 0.5 μmol L^{-1} NO_2^- and b, d, f, h for 5.0 μmol L^{-1} NO_2^-).
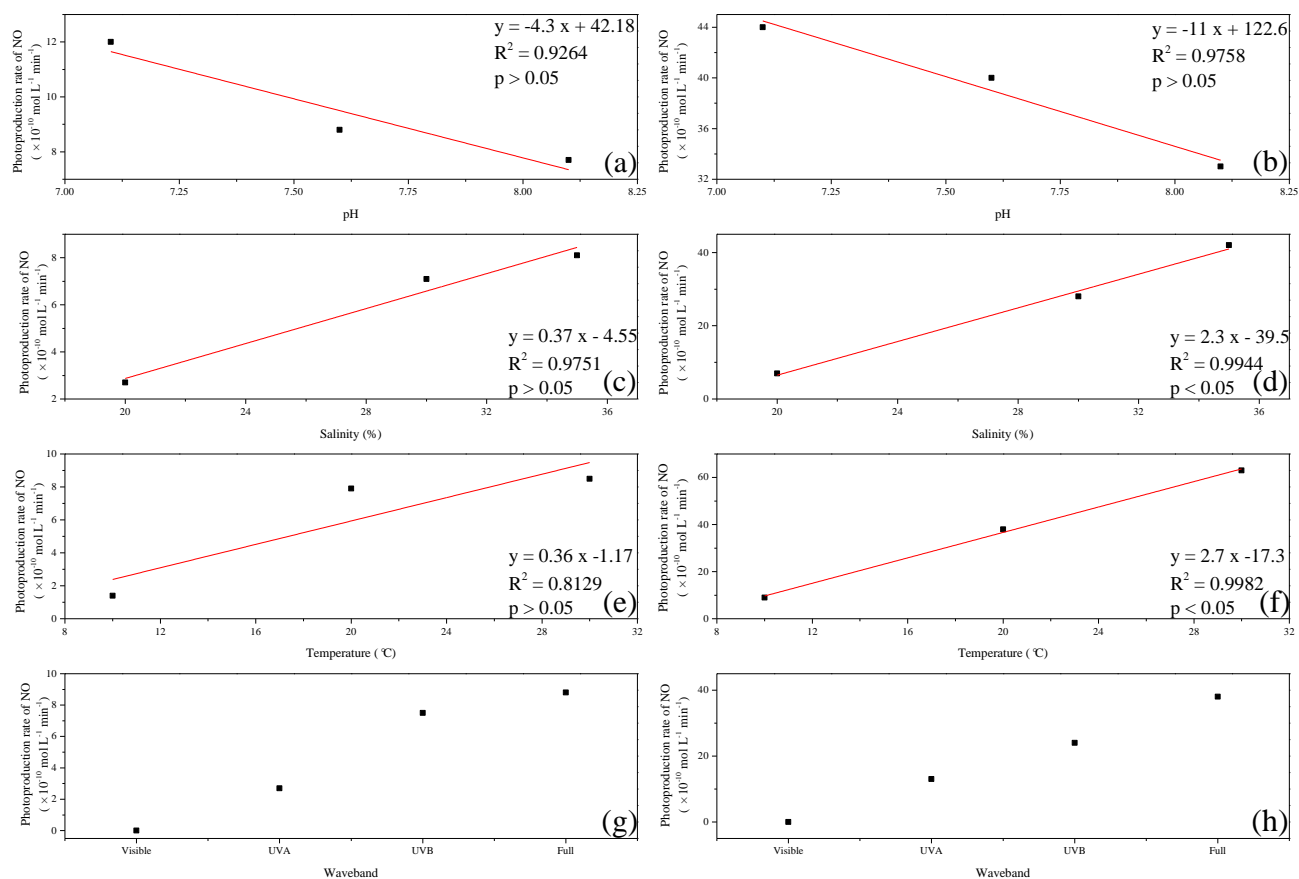
598

599

600

Fig. 5. Changes of NO photoproduction rates with irradiation time at different pH, salinity, temperature

and waveband conditions (a, c, e, g for 0.5 μmol L^{-1} NO$_2^-$ and b, d, f, h for 5.0 μmol L^{-1} NO$_2^-$).
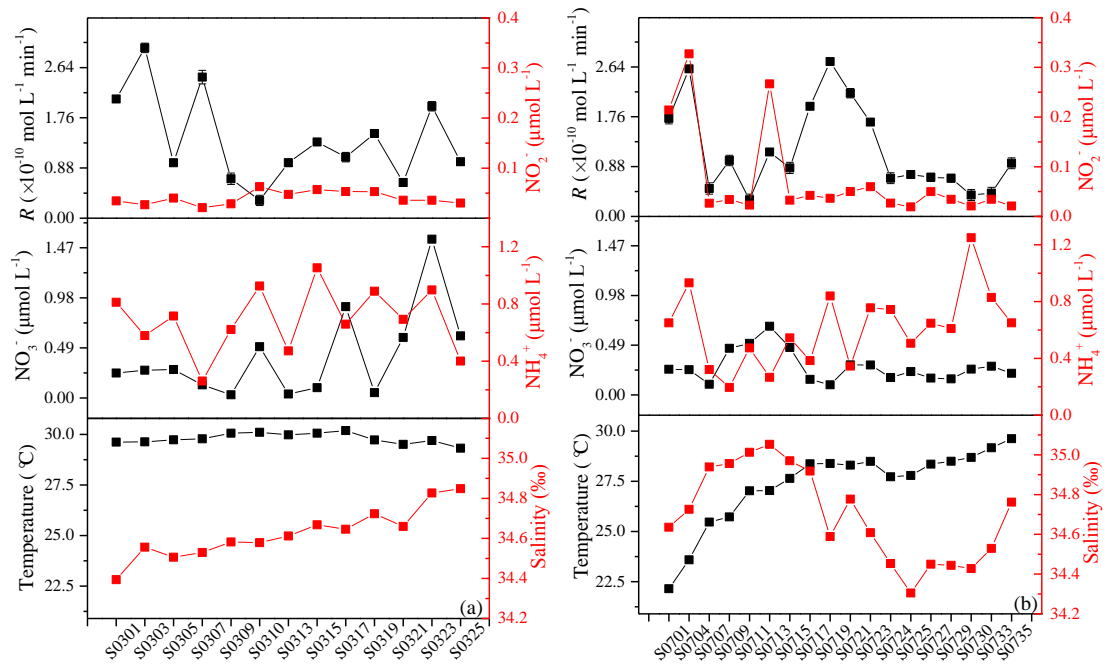
603

604

605 **Fig. 6.** Seawater temperature, salinity, concentrations of NO_2^-, NO_3^-, NH_4^+, and photoproduction

606 rates of NO (R_{NO}) in the western tropical North Pacific Ocean (a: W/E transect; b: N/S transect.).
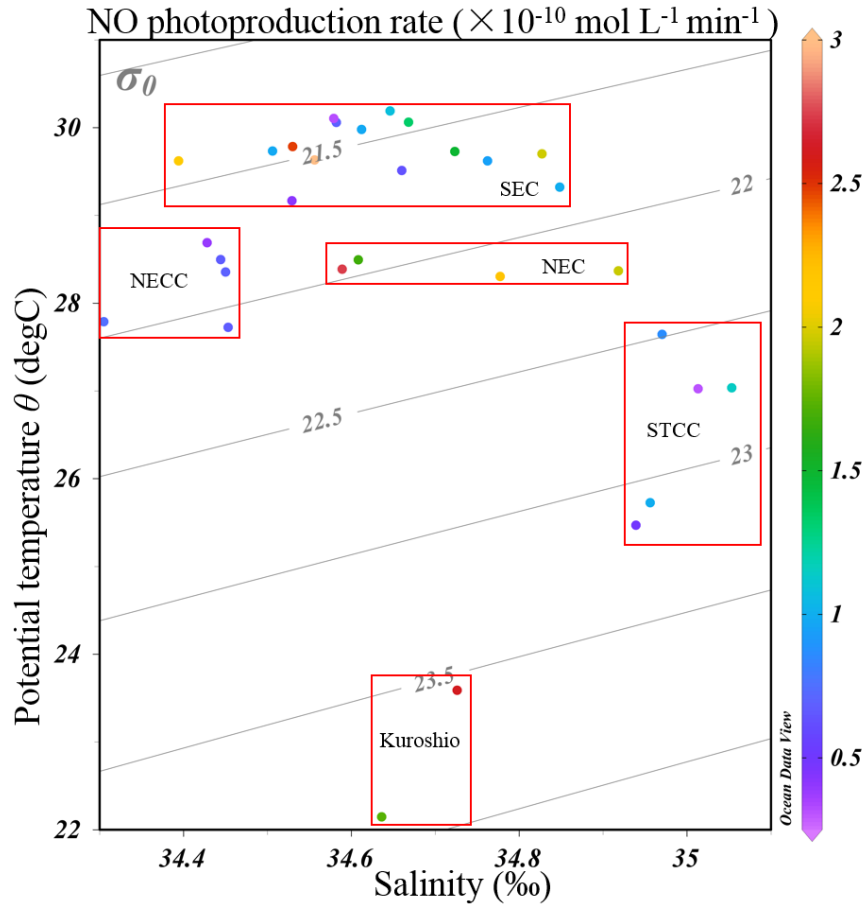
607

Fig. 7. The potential temperature–salinity (T–S) diagram with NO photoproduction rates indicated in the color bar. Water mass characteristics of the surface currents shown in Figure 1 are indicated. The acronyms NGCC, SEC, NECC, NEC, and STCC stand for New Guinea Coastal Current, South Equatorial Current, North Equatorial Counter Current, North Equatorial Current, and Subtropical Counter Current, respectively.

Table Captions

616 **Table 1** Photoproduction rates (R), average NO concentrations and average flux densities of NO in

617 different regions.

618 **Table 2** The ratios of photoproduction rates (R5.0/R0.5) in the different irradiation experiments.

619

620 **Table 1** Photoproduction rates (R), average NO concentrations, NO_2^- concentrations and average flux

621 densities of NO in different regions.

Regions	R (mol L^{-1} s^{-1})	NO (mol L^{-1})	NO_2^- μmol L^{-1}	Flux (mol m^{-2} s^{-1})	Sampling date	References
Seto Inland Sea, Japan	$8.7–38.8 \times 10^{-12}$	120×10^{-12}	0.5-2	3.55×10^{-12}	October 5–9, 2009	Olasehinde et al., 2010
Seto Inland Sea, Japan	$1.4-9.17 \times 10^{-12}$	$3-41 \times 10^{-12}$	0-0.4	0.22×10^{-12}	September, 2013 and June, 2014	Anifowose and Sakugawa, 2017
Kurose River, Japan	$9.4–300 \times 10^{-12}$	–	-	–	–	Olasehinde et al., 2009
Kurose River (K1 station), Japan	4×10^{-12}	1.6×10^{-12}	0.06	–	Monthly, 2013	Anifowose et al., 2015
Jiaozhou Bay	–	157×10^{-12}	-	7.2×10^{-12}	June, July and August, 2010	Tian et al., 2016
Jiaozhou Bay and its adjacent waters	–	$(160 \pm 130) \times 10^{-12}$	-	10.9×10^{-12}	March 8–9, 2011	Xue et al., 2011
Coastal water off Qingdao	1.52×10^{-12}	260×10^{-12}	0.75	-	November, 2009	Liu et al., 2017
Central equatorial Pacific	$> 10^{-12}$	46×10^{-12}	0.2	2.2×10^{-12}	R/V Knorr 73/7	Zafiriou and Mcfarland., 1981
The northwest Pacific Ocean	$0.5 \pm 0.2 \times 10^{-12}$	49×10^{-12}	0.06	1.8×10^{-12}	November 15, 2015 to January 26, 2016	This study

622

623 **Table 2** The ratios of photoproduction rates ($R5.0/R0.5$) in the different irradiation experiments.

	R ($\times 10^{-10}$ mol L^{-1} min^{-1})		Ratio
	0.5 μM	5.0 μM	
pH=7.1	12	44	3.7
pH=7.6	8.8	40	4.5
pH=8.1	7.7	33	4.3
T=10 ℃	1.4	9.0	6.4
T=20 ℃	7.9	38	4.8
T=30 ℃	8.5	63	7.4
S=20	2.7	7.0	2.6
S=30	7.1	28	3.9
S=35	8.1	42	5.2

624